UNIVERSITY OF GOTHENBURG

DEPARTMENT OF PHYSICS

SINGLE-PHOTON DOUBLE IONISATION OF ISOCYANIC ACID

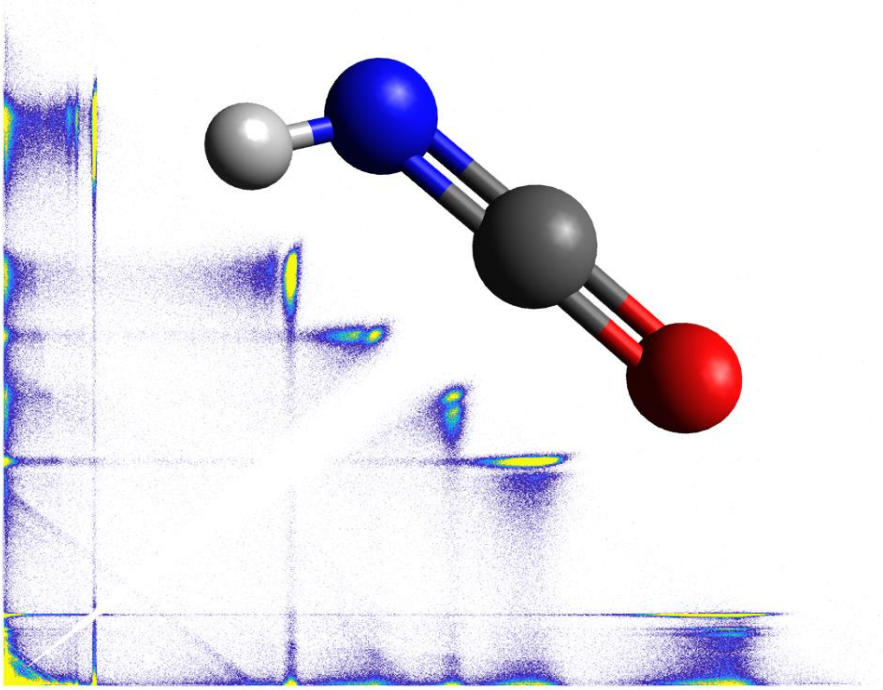

Viktor Axelsson
Ebba Johansson
Anthony Teichter

Degree project for Bachelor of Science with a major in Physics
2019, 180 HEC

Degree project for Bachelor of Science with a major in Physics

180 hec

Viktor Axelsson
Ebba Johansson
Anthony Teichter

Supervisor
Richard J. Squibb
Raimund Feifel

Deparment of Physics
Gothenburg University
Gothenburg, 2019

Abstract

Isocyanic acid (HNCO), a molecule containing the four most abundant atoms of organic chemistry, has been studied by single-photon double ionisation. Both direct double ionisation, such as core-valence and valence-valence ionisation, and indirect double ionisation processes, such as the Auger effect, were studied by ionising the molecule with photons in the extreme ultraviolet and soft X-ray spectral region produced with lab based light sources and the synchrotron radiation facility BESSY-II.

The spectroscopy method applied to these studies is based on a magnetic bottle electron spectrometer, by which the time-of-flight of the emitted electrons and their energy correlations were measured. For the Auger process, the photon energy is selected to be 20 eV above the threshold to ionise from the core shells of the molecule. The photon energies used to study the core-valence processes were selected so that there was sufficient energy to ionise a core and valence electron simultaneously. The onset energy of valence double ionisation was measured to be 32.0 eV with five resolvable peaks in the range 32.0-50.2 eV. The core-valence spectra are compared with the spectrum of single valence ionisation, while the onset of the Auger spectra are compared with the onset of the double valence spectra. These results motivate further experimental and theoretical studies into reactive, short-lived molecules.

Sammanfattning

Isocyanid syra (HNCO), en molekyl med de fyra främsta atomära byggstenarna inom organisk kemi, har studerats genom singelfoton dubbeljonisation. Både direkt jonisation såsom kärn-valens- och valens-valensjonisation och indirekta jonisationsprocesser såsom Augereffekten studerades genom att jonisera molekylen med fotoner i det extrema ultravioletta och mjuka röntgenspektrumet, producerat med labb-baserade ljuskällor och i synkrotronljusanläggningen BESSY-II.

Spektroskopimetoden som applicerats är baserad på en magnetisk flask-elektronspektrometer, som mäter flygtiden för utskickade elektroner och deras korrelerade energier. För att studera Augerprocessen valdes en energi som är 20 eV över tröskelenergin för jonisation från ett kärnskal av molekylen. Fotonenergin för kärn-valens valdes så att både en elektron från kärnskalet och en elektron från valensskalet kunde joniseras samtidigt. Tröskelenergin för dubbel valensjonisation uppmättes till 32,0 eV med fem urskiljbara toppar inom intervallet 32,0-50,2 eV. Spektrumet för kärn-valens jämförs med spektrumet för singeljonisation och tröskelenergin för Augerspektrumen jämförs med dubbelvalensjonisation. Resultaten motiverar djupare experimentella och teoretiska studier av reaktiva, kortlivade molekyler

Acknowledgements

We want to thank everyone that has helped guide us and answered all of our questions and our most sincere thanks to Måns Wallner for all his patience and guidance. We would also like to thank Jonas Andersson, Andreas Hult Roos and our supervisors Richard J. Squibb and Raimund Feifel.

Contents

List of Figures

List of Tables

1
Introduction

In 1838, Richard Laming, a British natural philosopher, proposed the concept of an indivisible particle with an electric charge, leading to J. J. Thomson and his team of physicists discovering the electron in 1897 [1, 2]. This was the beginning for new types of experiments involving the electron and the photoelectric effect. The photoelectric effect was discovered by Hertz and later explained by Einstein [3, 4]. Together with the work of Rutherford in 1914 the electron binding energies could be calculated with an equation in Rutherford's work [5].

During the 1920s the Auger effect was discovered independently by both Lise Meitner [6] and Pierre Auger [7]. The Auger effect was later used to explain the anomalies in the X-ray spectroscopy spectra. Lately this has become an analytic method, in form of Auger electron spectroscopy, used to distinguish chemicals and material surfaces. The field of photoelectron spectroscopy would advance forward after 1957 thanks to the contribution of Kai Siegbahn's work, also known as electron spectroscopy for chemical analysis [8].

Through Siegbahn's work it was made possible to study the atomic binding energies of core electrons. Simultaneously, D. Turner developed ultraviolet photoelectron spectroscopy with the purpose to study the valence electronic structure of molecules with a helium discharge lamp [9]. These techniques were the foundation of the work performed by John H. D. Eland together with his colleague Raimund Feifel, using a magnetic bottle spectrometer to study double photoionisation spectra of molecules [10].

Nowadays, electron spectroscopy is used in multiple fields of science to mostly study and characterise atomic and molecular structure, ionisation spectra, electron correlation of multiple photoionisation processes etc. A variant, which is used in this thesis, is photoelectron-photoelectron coincidence spectroscopy. Coincidence spectroscopy is a powerful analytic method for gathering information about the correlation of two or more emitted electrons, Auger decay processes, and the intensity distribution of doubly or more highly ionised final states.

1.1 Thesis outline

This thesis contains sections of the background of single and double photoionisation, relevance of coincidence measurements, introduction to TOF-PEPECO, shake-off and knock-out processes, the Auger effect and the synthesis of HNCO. There is also a review of the experimental set-up used in the lab in Gothenburg and at the synchrotron facility BESSY-II that includes: A helium gas discharge lamp,

synchrotron radiation, monochromators, mechanical chopper, magnetic bottle and MCP-detectors. This is followed by a chapter on data analysis, the presentation of the results obtained and conclusions.

2

Atoms and Molecules

The modern scientific description of the atom became possible with J.J Thompson's discovery of the first subatomic particle [2], the electron, together with Ernst Rutherford's experimental evidence of a small, positively charged nucleus. These discoveries lead to the Bohr model, illustrated in Fig. 2.1, where most of the atom is an empty void except for the orbiting electrons. The electrons and nucleus are tiny compared to the whole atomic system, and the whole atom is approximately 10,000 times larger than the nucleus [11].

2.1 Atoms

The structure of atoms can be a complex system where its electrons are located in different shells around the nucleus. Shown in Fig. 2.1 is an example of the oxygen atom. The number $n = 1,2,3...$ denotes the electron shell, and 1s, 2s 2p etc. are the subshells, where s and p refer to the orbital angular momentum.

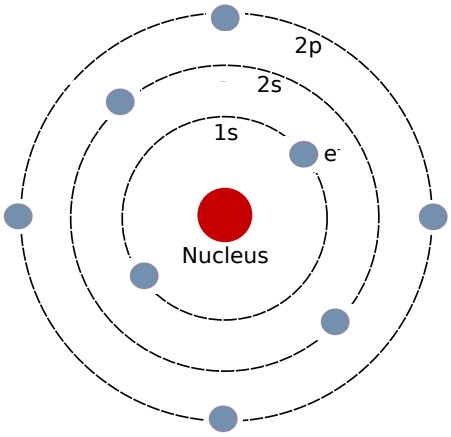

Figure 2.1: The oxygen atom. The positively charged nucleus in the centre with electrons orbiting the nucleus.

As seen in Fig. 2.1, there are two electrons in the 1s, two electrons in the 2s and four electrons in the 2p subshell. Each subshell is comprised of one or more orbitals with up to two electrons in each orbital. These orbitals have different shapes, shown as probability distributions in Fig. 2.2; the s-orbitals are spherically shaped and the p-orbitals have the shape of two lobes [12]. The two colours are representative of the sign of the wave function that defines the orbital. The electron configuration of the

oxygen atom can be denoted as $1s^2 2s^2 2p^4$ using the notation from Stoner [13]. The electrons located in the outer shells are most weakly bound to the nucleus, whereas those in the "core" (1s) shell are most strongly bound and require the most energy to remove.

2.2 Molecules

When two or more atoms combine to form a molecule, the energy level structure is much more complex than for the atom, due to the many different types of bonds that are formed and the fact that the vast majority interact with each other. Fig. 2.2 shows that when two 1s-orbitals constructively overlap they form a 1sσ-orbital, when two p_x- or two p_y-orbitals overlap they form a 2pπ-orbital, and when two p_z-orbitals overlap they form a 2pσ-orbital. This notation is used for the resultant molecular orbitals.

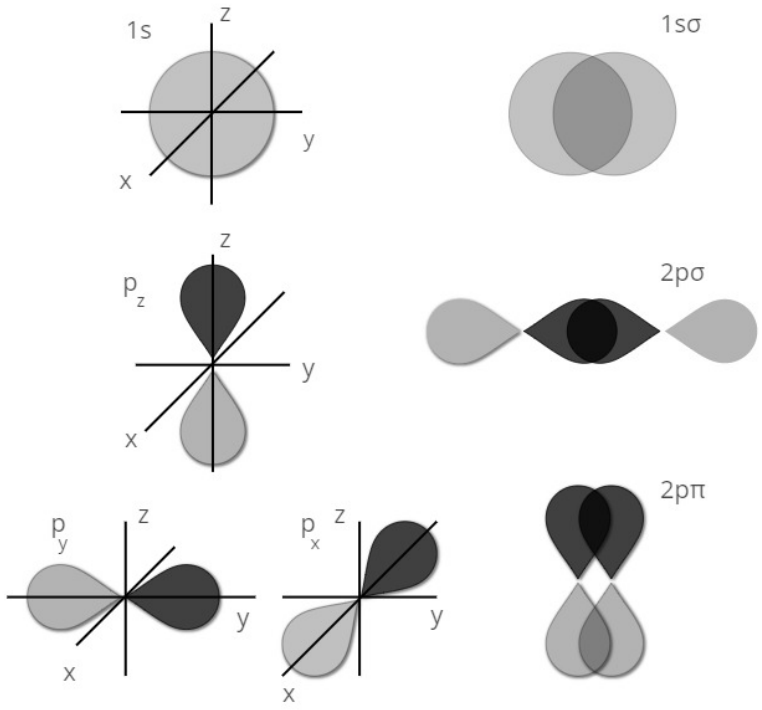

Figure 2.2: Visualisation of atomic s- & p-orbitals and molecular σ- & π-bonding orbitals. The two shades represent opposite signs of the wave function that defines the orbital. This figure was created in Vectr 2.0. [14].

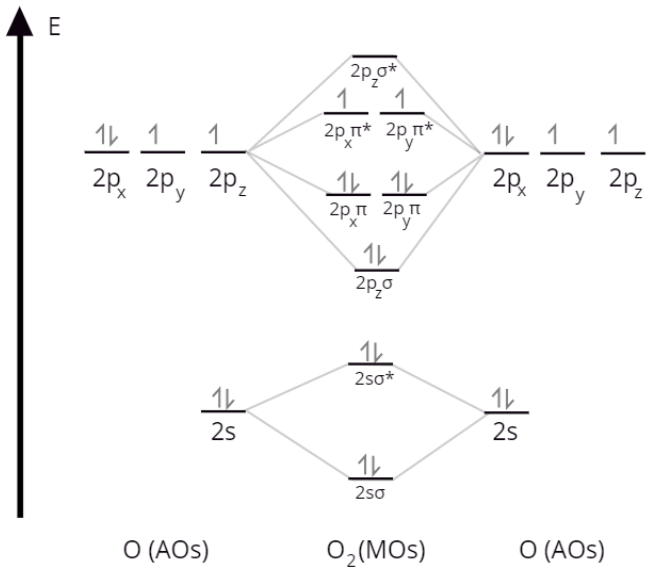

Figure 2.3: Schematic picture of how two oxygen atoms combine to form a molecule by the overlap of their atomic orbitals thus forming molecular orbitals. This figure was created in Vectr 2.0. [14].

In Fig. 2.3 we see how the atomic 2s- and 2p-orbitals of two oxygen atoms interact to form molecular oxygen. It is possible to see from the picture how this gives rise to a much more complex system than that of atomic oxygen. The electron configuration of O_2 can be denoted as

$$(1s\sigma)^2(1s\sigma^*)^2(2s\sigma)^2(2s\sigma^*)^2(2p\sigma)^2(2p\pi)^4(2p\pi^*)^2$$

where the asterisk symbol means the molecular orbitals are anti-bonding (in the case of destructive interference). This is just a simple example of the way atoms might bond together. Adding more atoms and creating more complex molecules will result in an abundance of different complex molecular orbitals, especially for the valence electrons of a large system. Deeper shells, however essentially retain an atomic-like energy structure since their orbitals are shielded from the effects of other atoms [15].

2.3 Isocyanic acid (HNCO)

This thesis presents studies of the molecule isocyanic acid (HNCO), discovered in 1830 by Liebig and Wöhler [16]. The HNCO molecule contains the four most abundant elements present in organic compounds, and the atoms are bound through covalent bonds, as seen in Fig. 2.4 [17].

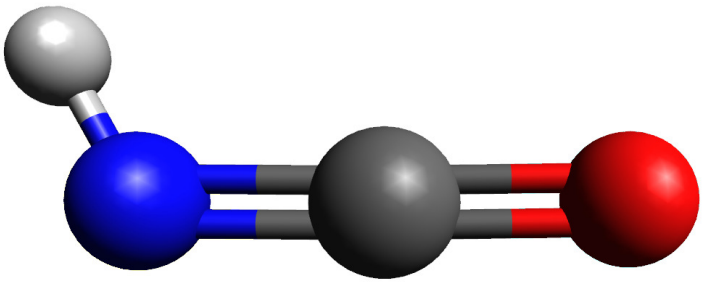

Figure 2.4: Isocyanic acid (HNCO). The HNCO molecule is bound by double covalent bonds between the C, O, and, N atoms and a single bond between the N and H atom. This figure was created in Avogadro [18].

The N, C, and O atoms each have different core 1s level energies which makes it possible to purposely select a certain photon energy to selectively ionise a targeted atom, and allows the study of processes occurring in one of the atoms within the molecule. In contrast, when ionising valance electrons, it is not so easy to study a specific atomic species due to the overlapping valence orbitals. Instead the valance ionisation of the molecule is studied as a whole [15, 19].

Knowledge of the core level energies and the valence spectrum of HNCO is a useful starting point for more complex studies. Thankfully, they have already been investigated by Eland in the 70s [20] and more recently by F. Holzmeier, et al. in 2018 [21]. The core ionisation energies for the C, N and O atoms are stated below in Tab. 2.1.

Table 2.1: The core ionisation energy of the different atoms in isocyanic acid [21].

	IE [eV]
C1s	295.9
N1s	405.7
O1s	540.2

The simple and yet diverse atomic composition of the molecule makes it a useful standard molecule for comparing experimental results with theoretical predictions. HNCO is a highly reactive and unstable molecule and has relevance in fields such as astrophysics [22], combustion reactions like RAPRENOx for removal of the toxic NO gases [23] and potential health risks [24]. Therefore there is a vast number of fields where experimental data on isocyanic acid might be of interest.

3

Photoionisation processes

In this chapter, an introduction to the spectroscopic techniques and a brief description of photoionisation will be given, followed by a discussion about single-photon multiple ionisation processes. The main focus is single-photon double ionisation, which can be achieved through both direct and indirect processes. For complex atoms or molecules, such as HNCO, both indirect and direct pathways exist [10].

3.1 Spectroscopy

Spectroscopy is the study of interactions between matter and electromagnetic radiation. The interaction between matter and electromagnetic radiation may generate a great number of processes. If the electromagnetic radiation is absorbed by the system, and the radiation has high enough energy, it may lead to emission of fluorescence, ejection of one or more particles or a combination of both. Different processes will produce different spectra and the aim of spectroscopy is to study and characterise them [10]. Spectroscopy can thus be performed in many different ways e.g. flame emission spectroscopy or particle spectroscopy. The method used in this thesis is photoelectron spectroscopy. A powerful method that is often used in combination with spectroscopy is coincidence analysis, which is explained in further detail in section 4.6.

3.2 Photoionisation

Experiments done by H. Herz in 1887 showed the existence of a light induced electrical current. He discovered that a charged object loses its charge faster when exposed to ultraviolet radiation due to the emission of electrons, contrary to what was believed from Maxwell's theory of light. The effect was later explained by Einstein in 1905, where he stated that energy is exchanged in discrete quanta [4]. He described the light as consisting of photons, which are particles defined as discrete quanta of the electromagnetic field.

Einstein formulated an equation for the photoelectric effect where the kinetic energy of the emitted electron equals the difference between photon energy and the work function. The photon energy is given by the product of Planck's constant and the photon frequency, $h\nu$, and the work function is defined as the energy required to remove one of the outermost electrons from the target. For free atoms and molecules, the work function is equal to the ionisation energy and Einstein's photoelectric effect

can be written as

$$\mathrm{KE} = \mathrm{h}\nu - \mathrm{IE}\,, \tag{3.1}$$

where KE denotes the electron kinetic energy and IE the ionisation energy. The IE corresponds to the binding energy of an electron in the atom or molecule, which is the lowest amount of energy required to remove the electron into free space. A photoelectron spectrum is created by plotting the photoelectron yield against its kinetic energy, and can show all possible electronic/vibrational states of the atom/molecule. The IE for every ionic state corresponds approximately to the orbital binding energy of the ejected electron. With the development of ionising light sources this technique was later made practically possible [10]. Such light sources used in this thesis are discussed in section 4.1.

3.3 Double photoionisation

Direct single-photon double ionisation is a process where a doubly charged ion is created when an atom or molecule absorbs one photon and emits two electrons, without an intermediate singly charged state being created. It is a one-step process with the two electrons emitted at the same time. The direct process can be written as

$$\mathrm{m} + \mathrm{h}\nu \rightarrow \mathrm{m}^{2+} + 2\mathrm{e}^{-}\,. \tag{3.2}$$

The direct process is forbidden by simple theory, where the electrons are assumed independent of each other, and is only made possible because of electron correlations. When the two electrons are emitted through a one-step process they will share the available excess energy arbitrarily according to

$$\mathrm{KE}_1 + \mathrm{KE}_2 = \mathrm{h}\nu - \mathrm{DIE}\,, \tag{3.3}$$

i.e. the energy that the outgoing electrons will share is the photon energy ($\mathrm{h}\nu$) subtracted by the double ionisation energy (DIE), where KE_1 and KE_2 are the kinetic energies for electron 1 and 2, respectively. The excess energy is distributed arbitrarily between the two electrons [10].

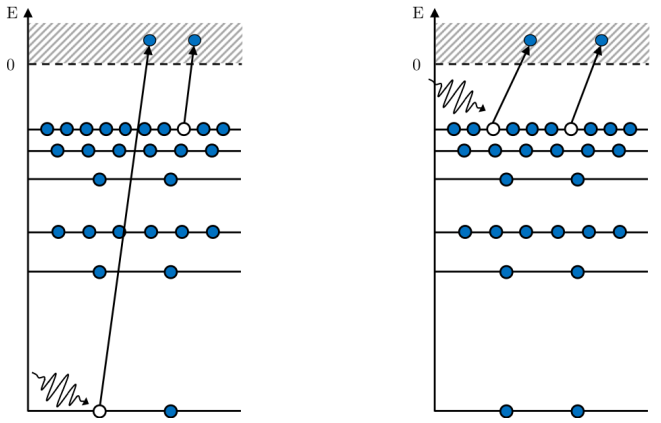

(a) Core-valence **(b)** Valence-valence

Figure 3.1: Two processes of single-photon direct double ionisation: core-valence (C-V) and valence-valence (V-V) ionisation. Pictures replicated with the permission of J. Andersson [25].

Double ionisation is often categorised by the orbitals the two emitted electrons come from, for example *core-valence* (C-V) and *valence-valence* (V-V) ionisation [25]. Both of these processes are shown schematically in Fig. 3.1a and 3.1b, respectively. To describe direct double ionisation there are two different models currently supported by theory and experiment, called knock-out (KO) and shake-off (SO) [10].

3.3.1 Shake-off

The SO mechanism is based on how the removal of one electron causes a sudden change in the residual ionic system, which can cause another electron to be ejected. It may also cause the second electron to be excited, which is then called *shake-up* [10].

The shake-off model is described purely as a quantum mechanical process. The model uses the sudden approximation where the primary electron escapes from the system instantly, without interacting with a second electron [25]. The primary electron leaving instantly will cause a sudden change in the Hamiltonian of the system [26]. This sudden change will cause the wave function of the second electron to collapse, which may lead to it being "shaken off" [25]. The shake-off mechanism becomes more probable higher the excess energy [26].

3.3.2 Knock-out

The KO model is based on an internal collision in the atom or the molecule. In this model a photon is absorbed, and tries to eject an electron. The photoelectron then interacts with another bound electron on its way out [10, 26]. In this interaction the primary electron will transfer some of its energy to the second electron, and the excess energy is hence shared between the two electrons so that both can escape the system [25]. The first electron has thus "knocked out" the second electron. The KO model is dominant for lower photon energies, near the ionisation threshold [10].

3.4 Auger effect

A doubly charged ion can also be created through/by indirect processes. In an indirect ionisation process, two consecutive ionisation events take place. The normal Auger effect, as shown in Fig. 3.2, is an example of this [6]. When the photoelectron is emitted a singly charged ion is created. If the photoelectron comes from an inner-shell, a vacancy is created which leaves the ion in an unstable, highly excited state. In order for the system to energetically relax the vacancy is filled by an electron from a higher shell, which releases energy. This is seen in Fig. 3.2. The energy may be released by fluorescence of a photon. Alternatively, the energy may instead cause one or more electrons to be emitted, creating a doubly or more highly charged ion. Furthermore, for heavier atoms with multiple core levels the ejected electron might leave the ion in another highly excited state causing further Auger decays, known as Auger cascade [27].

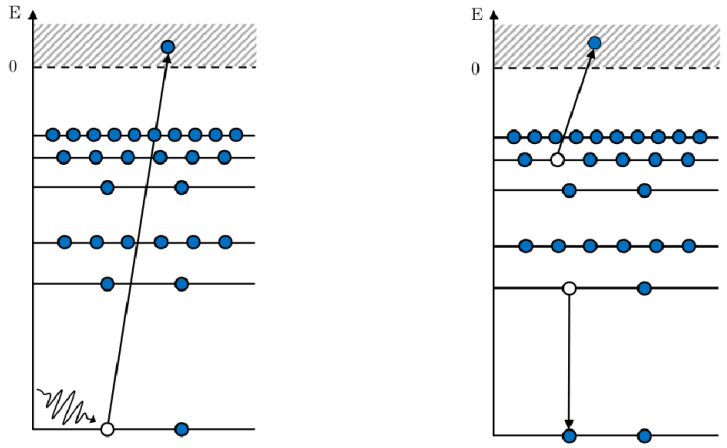

(a) Photoionisation process **(b)** Auger process

Figure 3.2: A photoionsation process where one photon emits one electron from the core, followed by an Auger process where the vacancy in the core is filled by an electron from a higher level, the energy released causes another electron to be emitted. Pictures replicated with the permission of J. Andersson [25].

When a doubly charged ion is created through this process the two emitted electrons will be at well-defined energies. There is therefore no smooth energy distribution as in the case of direct double ionisation. Instead, there will be discrete energy peaks. The peaks will be complementary though, since their sum must equal the difference between the photon energy and the energy of the final doubly charged state [10]. It is also noteworthy that the energy of the emitted Auger electrons are not dependent on the photon energy used, but are solely determined by the energy level structure of the target atom or molecule. The indirect processes, such as the Auger effect or fluorescent decay, are usually dominant over direct double ionisation processes [10].

4

Experimental Techniques

The experimental set-up, displayed in Fig. 4.1, is based on a method called *time-of-flight photoelectron-photoelectron coincidence spectroscopy* (TOF-PEPECO). To obtain reasonable resolution and exceptional collection efficiency over a wide range of energies, a magnetic bottle type electron spectrometer is used. In TOF-PEPECO spectroscopy a substance in the gas phase is ionised by a light source radiating at distinct energies, with the light sources used during these experiments radiating in the extreme ultraviolet and soft X-ray range. The collected data contains information about the time-of-flight (TOF) of the electrons, which is the time it takes for the electrons to travel a known distance. The time-of-flight is then converted into kinetic energy which can be used to determine the ionisation energies of the target substance [10].

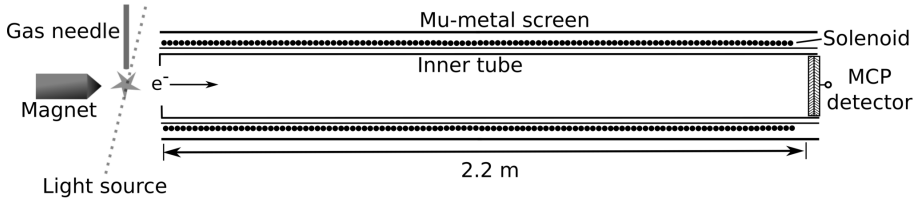

Figure 4.1: The spectrometer set-up as used in the Gothenburg lab. At BESSY-II a mechanical chopper discussed in section 4.3 was used. Picture replicated with permission of A. Hult Roos [28].

4.1 Light sources

It is common in spectroscopy to use light sources to either excite the system, break molecular bonds, or to ionise the system, the latter emitting electrons that can be used to study the electronic processes. The sources may range in complexity from a gas discharge lamp to a laser or a synchrotron radiation facility.

4.1.1 Helium gas discharge lamp

One way to obtain light in the ultraviolet range is to use a helium gas discharge lamp. The discharge lamp has a capillary filled with helium gas. A potential difference of several kV is applied across the capillary so that the gas becomes ionised. To make the gas discharge, the polarity of the potential is reversed rapidly, causing a short circuit. When the gas discharges it can emit light in the ultraviolet range at specific

photon energies. We focus on the characteristic He Iα (21.22 eV) and He IIα (40.81 eV) lines for the laboratory set-up [26].

The disadvantage of a helium discharge lamp is its limitations in available photon energies, which are limited to characteristic lines of the gases, and its much lower repetition rate (kHz) than that from a synchrotron radiation facility (MHz) [29].

4.1.2 Synchrotron Radiation

To produce synchrotron radiation it is common to use electron bunches (or other particles) that are accelerated to a relativistic speed in a storage ring. A magnetic field is used to bend the trajectory of the particles in a circular path. The electrons travelling along this path emit radiation along the tangent of the path every time the trajectory is bent.

The magnetic field is generated by three different types of devices: bending magnets, undulators and wigglers. The bending magnets, as implied by the name, bend the particles' path so that they will travel in a circular path with acceleration towards the centre of the orbit. The radiation emitted is shaped as a narrow cone directed tangentially from the path of the particle. The structure and principle of undulators and wigglers are similar to each other. Magnets are placed with alternating polarity in a periodic structure so that the particles travel in an oscillating trajectory, emitting radiation with each oscillation. The difference between undulators and wigglers is the strength of the magnetic field. The undulator produces low intensity radiation (soft X-ray) due to the lower amplitude of the oscillation process given by a weaker magnetic field. In contrast, wigglers produce high intensity radiation (higher than both undulator and bending magnets) since the amplitude of the oscillation is much greater, and thus the wavelength of the X-ray becomes shorter [30].

Synchrotron radiation at facilities like BESSY-II have many advantages when compared to laboratory environments since the intensity of the radiation can be controlled with high precision over a broad spectrum. It also has a high repetition rate, making them much more time efficient compared to using a helium gas discharge lamp [29]. The disadvantage is limited access compared to laboratory based light sources.

4.2 Monochromators

Light sources often radiate a broader spectrum than desired. To be able to select a specific photon energy from the radiation, a monochromator is often used. In the extreme ultraviolet to soft X-ray spectral region, monochromator functions in a way that the different wavelengths of the light are diffracted at different angles by a grating. The grating has periodic openings or etched lines in a substrate, with a constant distance (d) between them. The nth constructive interference for a reflective grating is then given by

$$d(\sin(\theta_{in}) + \sin(\theta_{out})) = n\lambda\,. \tag{4.1}$$

The photon energy is given by Planck's relation

$$\mathrm{E} = \frac{hc}{\lambda}\,. \tag{4.2}$$

Knowing the desired energy (E) and the incident angle θ_{in} it is easy to deduce at which angle the desired energy will be obtained.

The monochromators at synchrotron radiation facilities have to be able to function over a large photon energy range, and be insensitive to the thermal exposure of the radiation while still providing a precise energy operation, and are thus often considerably larger than monochromators in the optical region [26, 29].

4.3 Mechanical chopper

For measurements at a synchrotron storage ring facility the radiation is emitted with a very high light repetition rate (often MHz range). This repetition rate is much higher than what is appropriate for our set-up, since it does not allow the electrons created by one pulse to reach the detector before the subsequent pulse arrives. The window between pulses must be longer than the flight times of the slowest electrons, otherwise features coming from the next event may overlap with those from the previous event. To resolve this issue, a mechanical chopper was used, designed with two back-to-back rotating discs. In order to gain the desired frequency the number of slits on the disc is carefully matched to the rotation speed of the chopper and the synchrotron repetition rate, in this case having sets of either 120 and 15 slits. In rotating the discs relative to each other the width of their combined slit and opening time can be adjusted. The chopper is used to lower the pulse repetition rate to a range of $\sim$8 to $\sim$120 kHz [31].

The chopper is synchronised to the radio frequency signal of the single bunch of electrons orbiting the storage ring so that the pulses are transmitted consistently. This is important because the pulse intensity would otherwise vary significantly, giving a much lower average transmitted intensity. The maximum number of slits in the "rotating blade" that are used depends on the longest flight times and hence the length of the flight tube (so that the electrons will register on the detector before the next pulse gets through) [26].

The separation time between the bunches when operating in single bunch mode at BESSY-II is around 800 ns with a pulse duration of about 30 ps. In order for the chopper to not let two pulses of light pass through, the slits must be sufficiently small so that the full opening time is shorter than the bunch separation time [31].

4.4 Magnetic Bottle

The magnetic bottle is an electron TOF spectrometer designed such that the number of electrons detected by the spectrometer is maximised, and it is highly efficient when compared to more conventional TOF systems [32]. The name, "magnetic bottle", is illustrative of the effect it has on the electrons. A permanent magnet with a conical pole piece is placed so that it induces a strong magnetic field around

the sample, focusing the electrons towards the flight tube, along which a weaker magnetic field is induced by a solenoid wound around the flight tube, which guides the electrons towards the detector. The combination of the field lines generated by the permanent magnet and the solenoid becomes shaped like a bottle. An outline of how the magnetic field looks is shown in Fig. 4.2.

The electrons may be emitted from the sample in all possible directions, but the magnetic field guides them towards the flight tube according to the Lorentz-force [30, 33]

$$\mathbf{F} = q(\mathbf{E} + \mathbf{v} \times \mathbf{B}) \,. \tag{4.3}$$

The electrons will be highly affected by any interactions with other particles, making it necessary to perform such experiments under high vacuum and with the magnetic bottle to ensure that the electrons, that would otherwise often collide with either the flight tube or some other part of the spectrometer, are instead guided to the detector [26]. Our magnetic bottle yields almost 100% collection efficiency of ejected electrons, however the overall collection and detection efficiency of the instrument is about 50 - 60%, and is mainly determined by the efficiency of the detector. In comparison to more conventional spectrometers with an efficiency of a few percent, the magnetic bottle is much more time efficient and allows electrons with a wide spectrum of energies to be detected [10]. The resolution of the spectrometer is approximately the kinetic energy of the electrons divided by 50.

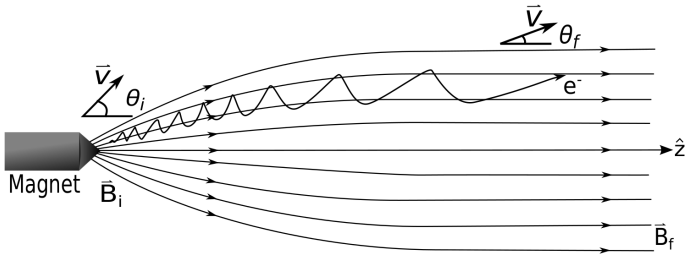

Figure 4.2: A schematic picture of the magnetic field that the magnetic bottle generates and the resulting flight path of the electrons. Picture replicated with permission of Andreas Hult Roos [28].

4.5 MCP-detector

A microchannel plate detector, or MCP, consists of plates with many ($\sim 10^6$) electron multiplier tubes with a very small diameter ($\sim \mu$m). The length of the tubes are also very short with the commercial standard ratio, $\frac{Length}{Diameter}$, between 40 and 120. The area of the plate annexed by these channels is at least 50 % of the total surface area of the plate. Each channel has a semi-conducting layer to which a high electric field is applied. When an electron hits the walls inside the channel it liberates one or more electrons, which are accelerated and in turn liberate even more electrons, eventually creating an avalanche of electrons. In this way, a single electron can be amplified by several orders of magnitude, yielding an electron pulse that can be measured with an anode [34].

In our experiment MCP-detectors are used to increase the detection and timing accuracy of our measurements. Our spectrometer has two to three MCPs mounted in a stack, which increases the amplification factor. The effect of the MCP has on the output is a pulse of about 10^8 electrons, which is further amplified and then fed into a fast time-to-digital converter (TDC) which can record the timing of the pulse with ns precision [10].

4.6 Coincidence measurements

Coincidence measurements aim to record two or more correlated particles from a single ionisation event. When an atom or a molecule absorbs a photon, one or more electrons might be ejected depending on what internal processes occur in the atom or molecule. If two electrons are ejected and originate from the same event their respective TOFs make it possible to distinguish their collective energies. Both electrons need to be detected in a specific time window before the next ionisation event takes place to be registered as coincidences, which of course also gives rise to both false coincidences from background noise and high ionisation rates. This is a challenge with the method and it is important to keep the false signals of coincidences as low as possible due to the low signal of true coincidences. The Poisson distribution can be used to describe the probability that a single light pulse ionises several species, and is formulated as

$$\mathrm{P}(n) = \frac{\lambda^n e^{-\lambda}}{n!}\,, \tag{4.4}$$

where n is the number of photoionisation processes and λ the average number of ionisations per light pulse [26, 29]. Minimising the false coincidence requires that the ionisation rates are low compared to the frequency of the ionisation source.

4.7 Synthesis of HNCO

The synthesis of isocyanic acid (HNCO) is through the basic reaction

$$\mathrm{C_{17}H_{35}CO_2H + KNCO \rightarrow C_{18}H_{35}KO_2 + HNCO}$$

where the mixing of the compounds stearic acid and potassium cyanate creates potassium stearate and the desired isocyanic acid as products. These reagents are solid at room temperature, however the melting point of stearic acid is 342.5 K which at this temperature forms a solution with the potassium cyanate. This solution is able to react and creates the product isocyanic acid and the byproduct potassium stearate.

Due to unwanted residual water in the reaction equipment there is another reaction which creates CO_2 by HNCO reacting with H_2O and also by the decomposition of HNCO. Any impurities in the sample will contaminate the spectrum with additional features that may overlap with the true spectrum of the sample, hence the sample must be purified (discussed in section 4.8). When condensing the sample,

some polymerises to form cyanuric acid, which is a polymer of the isocyanic acid monomer. It is seen as white powder in the vessel.

The main parts of the synthesis apparatus are the reaction vessel and the cold trap, where the cold trap condenses the product and ensures that the equipment remains at vacuum. The equipment is kept at vacuum to prevent possible contaminants or air reacting with the end product.

Lastly, HNCO has a boiling point at room temperature and it is a poisonous chemical, so the sample must be handled in a sealed environment [35].

4.8 Sample purification

Initially liquid nitrogen is used to quickly condense the sample leaving the sample to remain cold and kept solid for a longer period of time. In order to purify the sample from possible contamination of CO_2 we use a slush bath of CO_2 and Acetone [36]. The resulting temperature will be 196 K, which is about the same temperature at which CO_2 sublimates. By keeping the end products of the synthesis at this temperature HNCO remains a liquid with very low vapour pressure while CO_2 will rapidly sublimate. Due to the fact that CO_2 remains in gas form it will disappear significantly faster than the HNCO liquid when the sample is pumped under vacuum. This results in a purer sample, but with some loss of HNCO.

5
Data analysis

5.1 Time-to-energy conversion

In the TOF-PEPECO method the data received is in the form of counts listed with specific TOF for the electrons. The TOF directly relates to the kinetic energy (KE) of the electrons. The TOF can be converted to KE according to

$$\mathrm{KE} = \left(\frac{D}{t - t_0}\right)^2 + E_0\,, \tag{5.1}$$

where the parameters D, t_0 and E_0 are determined through calibration and are related to the length of the flight path of the electrons, a time offset between the ionising pulse and the start of the TDC clock, and an energy offset caused by electric fields in the spectrometer, respectively. The length of the flight path is determined largely by the length of the flight tube. These parameters remain constant for a given fixed experimental configuration, and can be calibrated as described in section 5.2, and the parameters for the calibration of the data from the Gothenburg lab and BESSY-II are presented in section 6.1.

The TOF is measured in intervals of 1 ns, which for higher electron energies may correspond to a large energy difference due to the nonlinear nature of eq. (5.1). When trying to convert the TOF data to energy this imprecision may cause discontinuities in the data. One way to resolve this problem is to generate a randomised time distribution for the electrons within each 1 ns interval to fill the "gaps" in the energy spectrum.

5.2 Calibration

The calibration is done to determine the unknown parameters in eq. (5.1). The calibration is preferably done using single ionisation spectra of a well-known sample that has sharp peaks and covers the same energy range as the data that will be collected [10]. Molecular oxygen has a large number of peaks at lower binding energies and is therefore used in the Gothenburg lab with the photon energies 21.22 and 40.8 eV. Argon is used at BESSY-II since it has sharp atomic lines at higher binding energies, which are better suited for BESSY-II's photon energy range.

The measured TOF for the electrons relates to their KE which in turn equals the difference between the photon energy and the ionisation energy, according eq. (3.1). Since the samples used for calibration have well-known photoelectron spectrum and

knowing the photon energy $h\nu$, in eq. (3.1) it is possible to map the TOF peaks to their specific ionisation energies. The calibration is done by fitting the TOF values of the peaks to eq. (5.1).

5.2.1 Oxygen

In the Gothenburg lab molecular oxygen (O_2) is used for calibration. The valence spectrum of oxygen [37] is well characterised and has a large number of resolvable electronic and vibrational states, which makes it well suited for calibration. Oxygen is mainly used for calibrating when low level energy radiation is used as the source of ionisation. The characteristic spectral lines of oxygen along with their corresponding assignments are given in Tab. 5.1 [37].

Table 5.1: Energies for specific orbitals of O_2 used for the calibration of data obtained in the Gothenburg lab. Orbitals for which the vibrational states are resolvable have multiple energies listed.

Oxygen orbitals	IE [eV]
$X^2\Pi_g$	12.30
$a^4\Pi_u$	16.62
$b^4\Sigma_g^-$	18.171
	18.315
	18.454
$B^2\Sigma_g^-$	20.296
	20.433
	20.563
	20.69
	20.812

5.2.2 Argon

At BESSY-II argon is used as a calibration sample. It is used in a similar fashion as for oxygen but is better suited for higher photon energies where the valence spectrum of O_2 becomes unresolvable. Although only the two 2p photoelectron lines in argon are used for the calibration, there will still be many measured TOFs to calibrate from, since the synchrotron radiation at BESSY-II allows us to tune the photon energy and therefore the kinetic energy of the 2p electrons.

Table 5.2: Ionisation energies for the different orbitals of argon [38]; orbitals in boldface are the ones used for calibration.

Argon orbitals	IE [eV]
L_1 2s	326.3
$\mathbf{L_2}$ $\mathbf{2p_{1/2}}$	250.6
$\mathbf{L_3}$ $\mathbf{2p_{3/2}}$	248.4
M_1 3s	29.3
M_2 $3p_{1/2}$	15.9
M_3 $3p_{3/2}$	15.7

5.3 Coincidence analysis

When two electrons are registered in the same time window they are considered to originate from the same event [29]. Their respective TOFs or their TOFs converted to energy, can be studied in a coincidence map. In a coincidence map it is possible to see the electron correlation of direct double ionisation, or indirect processes, such as the Auger effect. There are many ways to plot the coincidence map. One way is to have both axes in the kinetic energy domain, where the axes will represent the kinetic energy of the electrons respectively.

The events where a direct double ionisation takes place will form a diagonal line in the coincidence map in the energy domain, due to the arbitrary energy sharing. The Auger electrons will be vertical/horizontal lines or distinct islands in the coincidence map because of their fixed kinetic energies; this results in features that are parallel to one of the two energy axes. An example of how the direct double ionisation and Auger processes can look in a coincidence map in KE space can be seen in Fig. 5.1.

With the same data it is also possible to obtain a DIE spectrum. The DIE equals the photon energy minus both of the electrons, KE, as shown in eq. (3.3). A coincidence map can be created if the DIE is plotted on one axis and the single electron KEs for both electrons on the other axis. The projection of this map onto the axis with the DIE then yields a DIE spectrum.

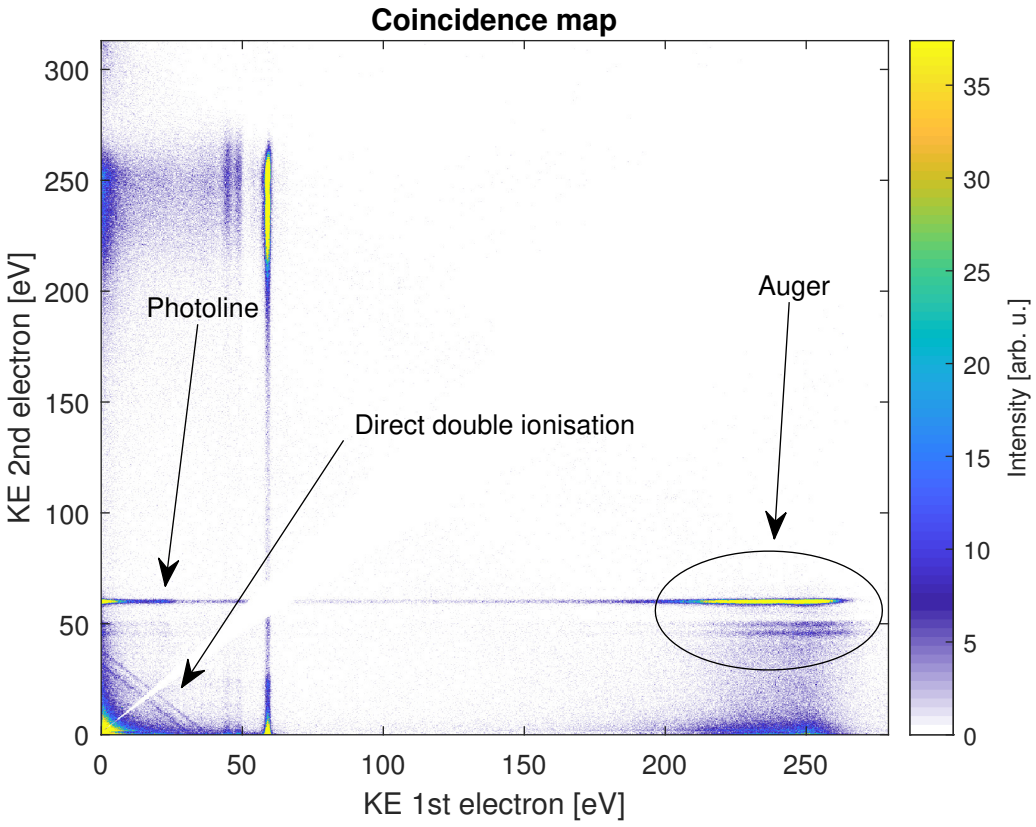

Figure 5.1: A picture indicating where in the coincidence map direct double ionisation and Auger processes can be seen, illustrating their distinctive shapes.

6
Results & Discussion

6.1 Calibration

The calibration parameters, from section 5.1, are calculated using a fit function in MATLAB, and are then used to convert the data from the TOF to the energy domain. The parameters obtained using molecular oxygen in the Gothenburg lab and atomic argon at BESSY-II, are given in Tab. 6.1. The fitted functions and the data used for the calibration are shown in Fig. 6.1. Fig. 6.1a shows the calibration for the lab data from Gothenburg and Fig. 6.1b for the BESSY-II data. The raw spectra that provide the calibration data for different photon energies for both oxygen and argon in the TOF domain are seen in Fig. 6.2a and Fig. 6.2b, respectively. A higher photon energy results in a higher KE and therefore a shorter TOF, which is why the peaks are shifted in the plots. One can also see in Fig. 6.2 that a lower photon energy, and hence lower kinetic energy electrons, yields better resolution. With lower photon energies there are two clearly visible peaks, and as the photon energy increases, the time between the two peaks decreases, and they eventually blend together.

Table 6.1: Fitted calibration parameters used to convert between time-of-flight and energy, for both the Gothenburg Lab and BESSY-II set-ups.

	D [$\sqrt{\text{eV}}$ns]	t_0 [ns]	E_0 [eV]
Parameters for BESSY-II	3681.4	33.6	-0.5
Parameters for the Lab	3736.7	37.3	0.3

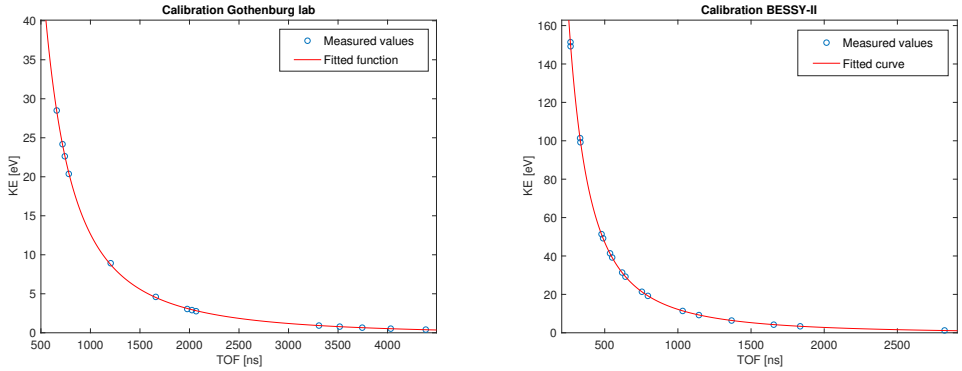

(a) Molecular oxygen **(b)** Atomic argon

Figure 6.1: The fitted functions of molecular oxygen for the Gothenburg lab (a) and of atomic argon for BESSY-II (b). For comparison, the measured time-of-flight and kinetic energy values, which the functions are fitted from, are plotted as well.

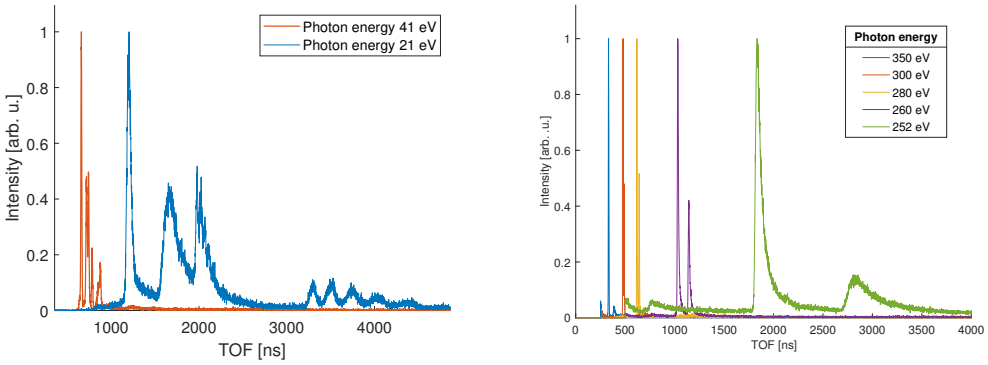

(a) O_2 spectra **(b)** Argon spectra

Figure 6.2: The spectra of molecular oxygen (a) and atomic argon (b) for different photon energies, used to fit the calibration parameters. The spectra are plotted on the TOF scale.

6.2 Purification checks

Fig. 6.3 shows the valence spectra for HNCO before and after purification, where, Fig. 6.3a shows the Gothenburg lab data and Fig. 6.3b the BESSY-II data. For the data from BESSY-II, the electrons were retarded by approximately 78 eV by applying a voltage to the flight tube so the kinetic energies matched those obtained in the laboratory set-up. A peak can be seen around 13.9 eV in both cases and another peak can be seen at 18.1 eV in Fig. 6.3a. These peaks originate from CO_2 and disappear after purification, which indicates that the sample contains nearly pure HNCO and therefore CO_2 is less likely to interfere with the experiment.

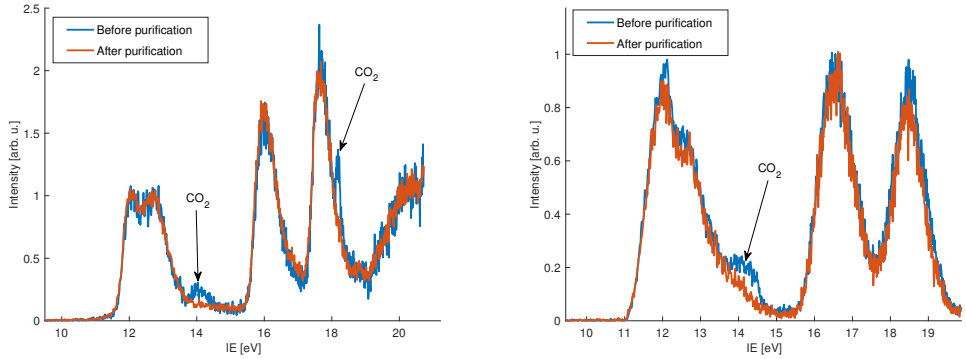

(a) **(b)**

Figure 6.3: Valence photoelectron spectra of HNCO before and after purification in the Gothenburg lab (a) obtained at the photon energy 21.22 eV and at BESSY-II (b) obtained at the photon energy 100 eV. The peaks that disappear after purification are CO_2. The electrons at BESSY-II were retarded by approximately 78 eV.

6.3 Single Ionisation

In Fig. 6.4 the spectra for single valence ionisation at the photon energies 21, 41 and 90 eV can be seen. The ionisation energies of the peaks observed are given in in Tab. 6.2. This spectrum matches that obtained by high resolution photoelectron spectroscopy by Eland [20]. The resolution is lower in our case and, as mentioned before, the resolution decreases when the electrons have a higher KE, which is the case for higher photon energies.

Table 6.2: Single ionisation energies (IE) of HNCO. The values for the different peaks are derived from the spectra for the lowest possible photon energy, where the resolution is best.

Single ionisation peaks					
IE [eV]	11.3	12.1	15.6	17.4	20.0

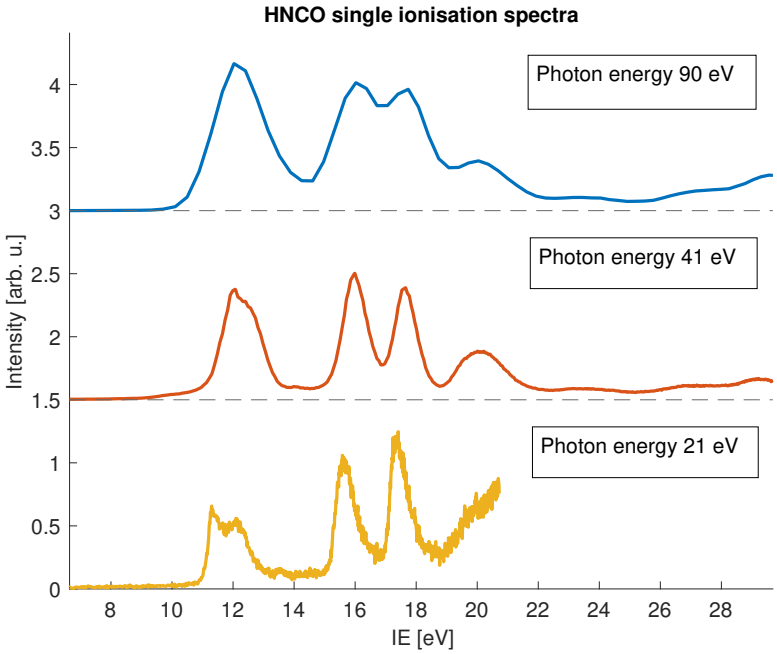

Figure 6.4: Single photo ionisation spectra of HNCO obtained at different photon energies. The resolution deteriorates at higher photon energies.

6.4 Valence-valence direct double ionisation

The valence-valence double ionisation process can be seen in coincidence maps in the TOF domain in Fig. 6.5, in the KE domain in Fig. 6.6 and in KE versus the DIE in Fig. 6.7. In the latter plot, the energies of the two single electrons are plotted against the DIE. In energy space, four straight lines representing the double ionisation can be seen, which manifest as hyperbola in the TOF domain. The four valence-valence lines might not be visually obvious in the TOF domain due to their low TOFs, but are clearly visible in both the KE domain (Fig. 6.6) and in the related DIE map (Fig. 6.7).

In Fig. 6.8 the double ionisation spectra for the photon energies 41, 90 and 100 eV are shown. The DIE range is cut because of DIEs lower energy are unphysical. The ionisation potential is approximately 11 eV, therefore it is not possible to have any double ionisation with less than twice this energy. The first peak appears at the DIE 34.0 eV, with the onset at 32.0 eV, and the second peak at 38.7 eV. When comparing the spectrum for 41 eV with the spectra for 90 and 100 eV, the peak at 38.7 eV is resolvable only for the higher energies while the second visible peak at the end of the spectra for 41 eV is due to noise. All the noise seen in the TOF space for long TOFs of the electrons will be bunched together in KE space at very low kinetic energy, and this noise will increase for higher ionisation energies and hence appear as enhanced intensities at higher ionisation energies. There are additional peaks visible using the higher photon energies of 90 and 100 eV, since the DIEs for these peaks are higher than 41 eV. However the resolution for these peaks are quite low due to the increased KE, making them less resolved. The DIEs of all the

identifiable features are summarised in Tab. 6.3

Table 6.3: The DIE for the V-V double ionisation. The three last peaks have low resolution, making their values quite approximate.

V-V double ionisation peaks					
DIE [eV]	34.0	38.7	42.7	45.0	50.2

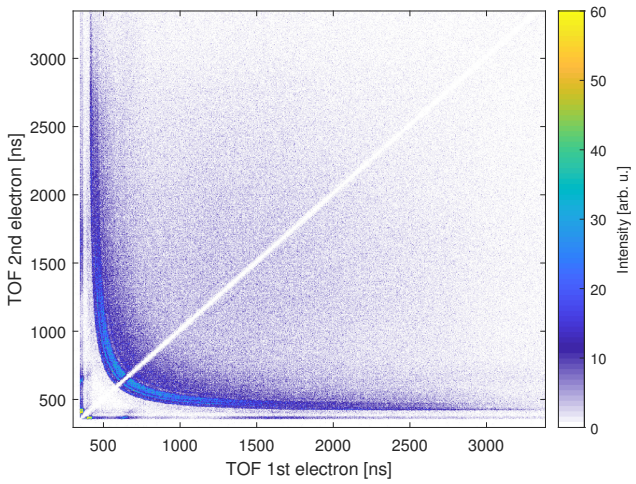

Figure 6.5: Coincidence map of HNCO for both detected electrons in the time-of-flight domain, obtained at photon energy 100 eV.

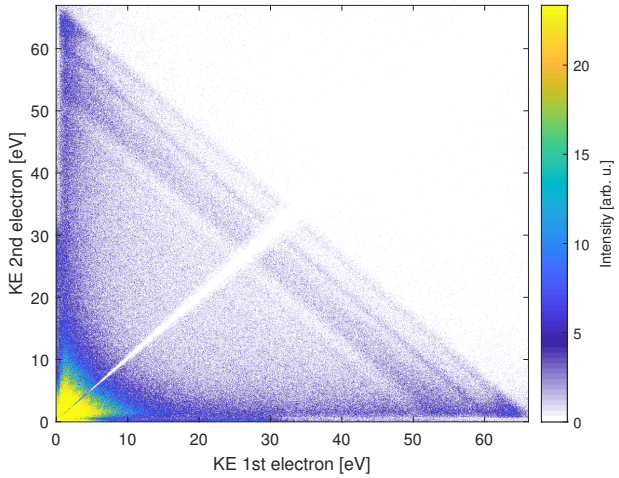

Figure 6.6: Coincidence map of HNCO plotting the kinetic energy of both detected electrons, obtained at photon energy 100 eV.

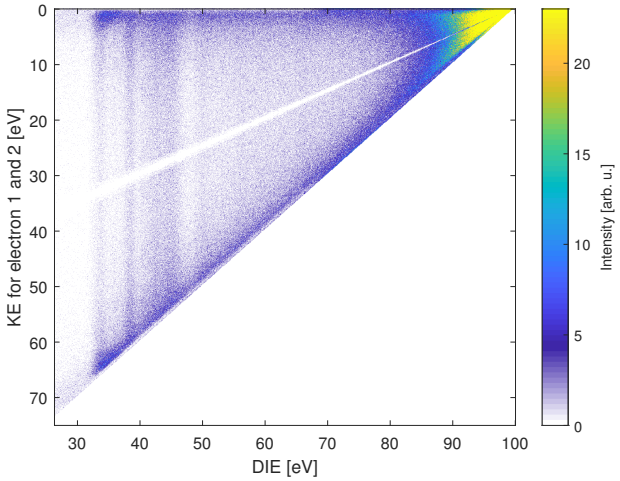

Figure 6.7: Coincidence map of two detected electrons, obtained at photon energy 100 eV. The horizontal axis reflects the ionisation energy and the vertical-axis single electron kinetic energy of both electrons.

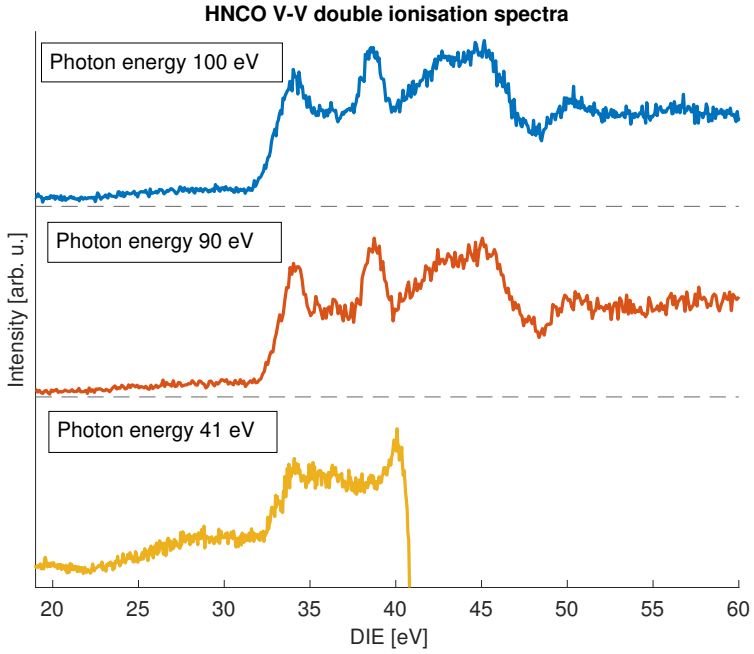

Figure 6.8: Double ionisation spectra of HNCO with scaled intensities, for the photon energies of 41, 90 and 100 eV.

6.5 Core-valence direct double ionisation

To doubly ionise HNCO by removing a core electron and a valance electron, three different photon energies were used: 356 eV, 466 eV and 600 eV. These photon energies are selected so that the core electron will originate from a different atomic species in each case. When using the photon energy 356 eV the core electron comes

from carbon 1s-orbital (C1s), with the photon energy 466 eV it comes primarily from the nitrogen 1s-orbital (N1s) and with the photon energy 600 eV it comes primarily from the oxygen 1s-orbital (O1s). In addition, these energies are chosen so that they are equally above the corresponding inner shell threshold energies listed in table 2.1, namely 60 eV, with the expectation that the core valence features will appear at energies less than 40 eV.

The fact that the photon energy used is equally above the threshold in each case means that the excess energy of the electrons will be roughly the same for all cases. This can be seen when comparing the coincidence maps in Fig. 6.9, 6.10 and 6.11 which reflect the core-valence process involving C1s-, N1s- and O1s-orbitals, respectively. The coincidence maps look similar to each other and the diagonal lines, which correspond to the core-valence double ionisation, have similar energy distributions in the three cases. In the coincidence maps there are two clear lines and one faint. The same lines can be seen as peaks in Fig. 6.12, where the core-valence double ionisation spectra can be seen. For the C1s-orbital there are three peaks, for N1s there are two peaks and for O1s there are three peaks. All of their DIEs are summarised in Tab. 6.4. The spectra shown in the figure are shifted in energy so that the first visible states are aligned.

Table 6.4: The DIEs for C-V. The values are obtained from the lowest possible photon energy, where the resolution is the best.

C-V double ionisation peaks			
C1s DIE [eV]	317.8	321.8	323.8
N1s DIE [eV]	429.6	434.2	
O1s DIE [eV]	561.6	567.5	569.9

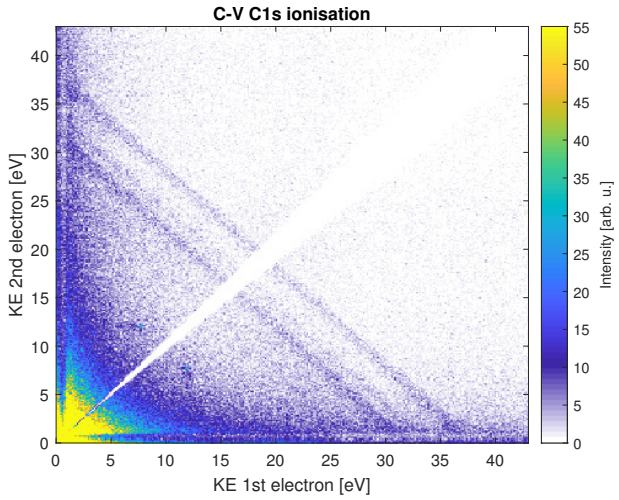

Figure 6.9: Electron kinetic energy coincidence map of HNCO obtained at photon energy 356 eV. Core-valence ionisation from the C1s-orbital can be seen as the diagonal lines for electron energy sums below 40 eV.

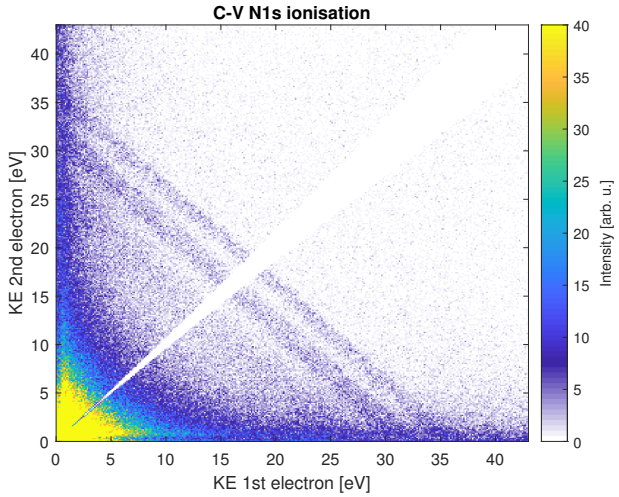

Figure 6.10: Electron kinetic energy coincidence map of HNCO obtained at photon energy 466 eV. Core-valence ionisation from the N1s-orbital can be seen as the diagonal lines for electron energy sums below 40 eV.

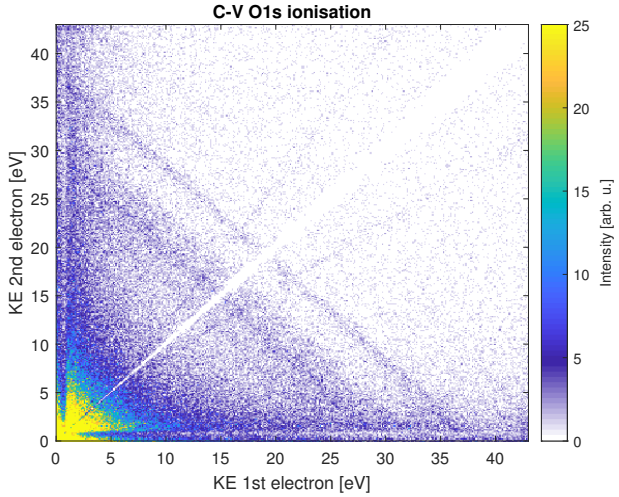

Figure 6.11: Electron kinetic energy coincidence map of HNCO obtained at photon energy 600 eV. Core-valence ionisation from the O1s-orbital can be seen as the diagonal lines for electron energy sums below 40 eV.

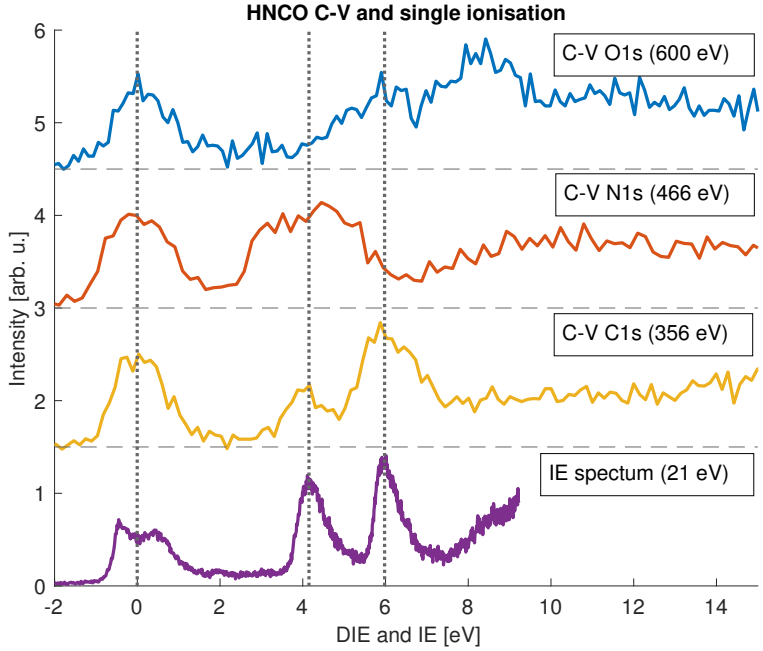

Figure 6.12: The top three spectra show core-valence spectra involving the C1s, N1s and O1s shells, which are compared to the single valence ionisation spectrum (bottom spectrum). The intensity of the spectra has been scaled to be comparable to each other. The spectra are shifted in energy so that the centre of the first peak of each spectrum is at 0 eV.

The valence single ionisation spectrum is also plotted in Fig. 6.12 underneath the three core-valence spectra. It is interesting to compare the final states for core-valence and valence single-ionisation because, even though the core and valence electron may influence each other in the process, the influence they have on each other has minimal impact on the energy of the initial and final state. This means that the structure of the core-valence spectra are expected to have similar features to those of the single valence spectrum, but with a significant offset in energy that will correspond to the energy required to eject the core electron and the interaction of the core and valence electrons. From Fig. 6.12 it is possible to see that the structure of the spectra looks similar for C-V and single valence.

The C-V spectrum that most resembles the single ionisation spectrum is that for C1s. In Fig. 6.13 the spectrum for C1s is plotted above the energy shifted spectrum for the single ionisation. The energy shift between the two spectra is 306 eV, which yields the core-valence interaction energy of $\sim$ 12 eV for carbon. From J.H.D. Eland's work it is possible to assign valence states to the peaks for the two spectra [20]. These states can be seen in the Fig. 6.13, labelled with the same notation as used by Eland.

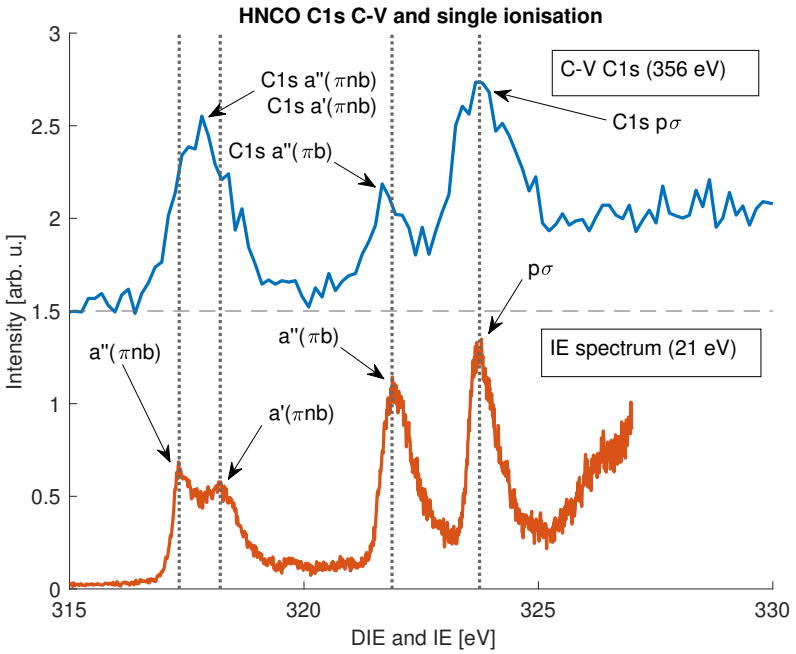

Figure 6.13: Core-valence spectrum for the C1s shell and the single ionisation spectrum. The intensity of the spectra have been normalised. The single ionisation spectrum has been shifted by 306 eV to align with the C-V spectrum. The notation of the valence states is from J.H.D. Eland's work [20].

6.6 Auger spectra

The Auger process can be seen as islands in the coincidence maps in Fig. 6.14a, 6.15a and 6.16a, as discussed in section 3.4. In addition, the figures show one electron with high KE and another one with a low KE. The electron with lower energy is ejected from the initial core ionisation and the one with higher energy is a result of the Auger relaxation ejecting a valence electron. The photon energy is selected to be around 20 eV above the threshold for the 1s ionisation.

The photoelectrons and the Auger electrons are correlated, which means that they will be detected as a single event. This results in an enhanced intensity, which will appear as an island in the coincidence map because of the fixed energies, as mentioned in section 5.3, with the KE of the photoelectron on one axis and the KE of the Auger electron on the other. This also gives rise to islands that correspond to states called satellites, which are products of different possible excitation and relaxation pathways in the atom. In the coincidence maps 6.14a, 6.15a and 6.16a we see that the intensity of the main photoelectron line correlated Auger feature has a higher intensity than the satellites, which is expected since satellite states are generally weaker than the main state. It is also possible to extract full and partial Auger spectra by selecting a limited region of the map and integrating over all photoelectron energies. These extracted Auger spectra are shown in Fig. 6.14b, 6.15b, and 6.16b. We can also see that the main photoelectron line has more pronounced features than that of the satellites. In addition, we see resemblance between the

features we obtain and those published by F. Holzmeier et al. [21].

The onset energy of the final doubly ionised states, shown in Fig. 6.17, 6.18 and 6.19, for the three core vacancies are at approximately the same energy. The onset of double ionisation most closely matches that extracted for V-V for the carbon Auger spectrum, while for nitrogen and oxygen there are larger discrepancies. The discrepancies may be due to the resolution of the spectrometer that becomes lower for higher KE electrons, which is the case for nitrogen and oxygen due the high KE of these Auger electrons.

The shapes of the distributions vary and this difference originates from the route taken between the photoionisation step and the final state. The route can involve direct double ionisation processes, Auger processes, charge transfer within the molecule and molecular fragmentation processes; all of these processes affect the distribution. The probability to end up in a particular doubly ionised state differs for each route, and is why the Auger DIE and the V-V DIE appear to differ.

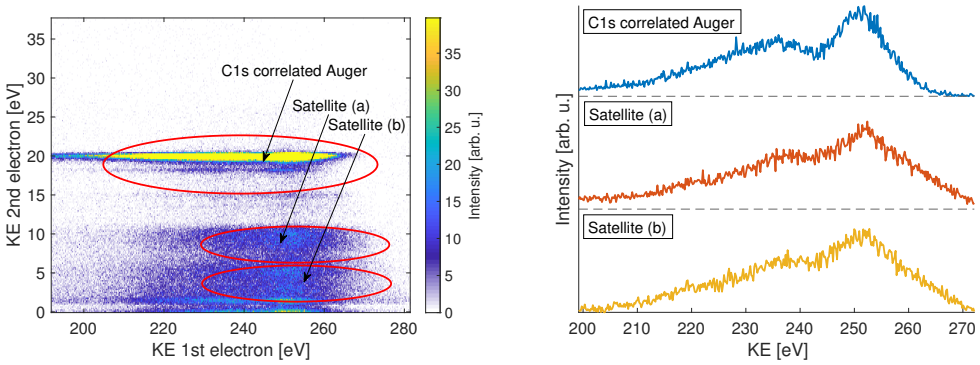

(a) Coincidence map **(b)** Intensity against KE

Figure 6.14: The figure to the left (a) shows Auger electrons in coincidence with the C1s photoelectrons. The figure to the right (b) shows the correlated intensities respectively to the areas marked in (a), plotted in KE space. The data was obtained using the photon energy 316 eV.

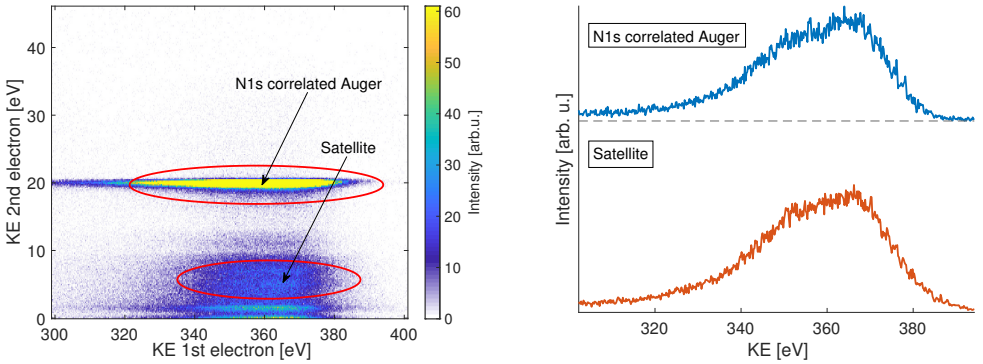

(a) Coincidence map **(b)** Intensity against KE

Figure 6.15: The figure to the left (a) shows Auger electrons in coincidence with the N1s photoelectrons. The figure to the right (b) shows the correlated intensities respectively to the areas marked in (a), plotted in KE space. The data was obtained using the photon energy 426 eV.

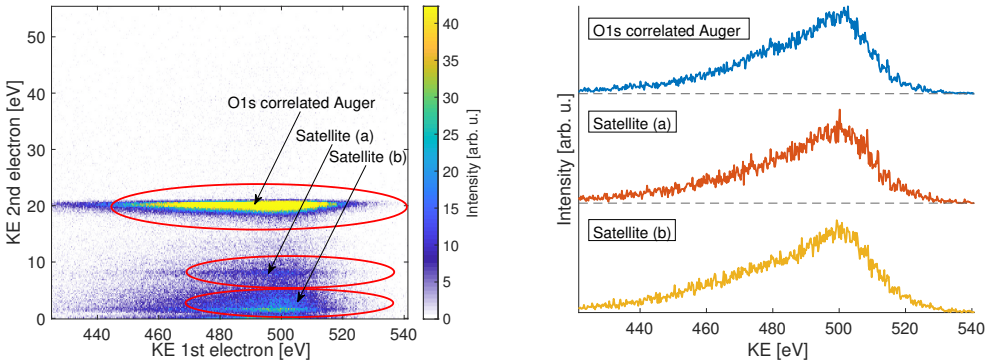

(a) Coincidence map **(b)** Intensity against KE

Figure 6.16: The figure to the left (a) shows Auger electrons in coincidence with the O1s photoelectrons. The figure to the right (b) shows the correlated intensities respectively to the areas marked in (a), plotted in KE space. The data was obtained using the photon energy 560 eV.

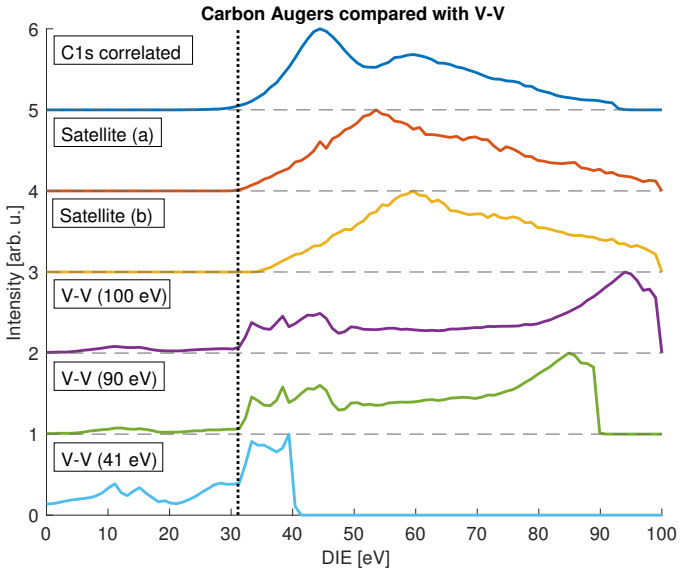

Figure 6.17: Comparison of the double ionisation spectra of the carbon Auger electrons and the valence-valence double ionisation spectra with a dotted line located at the onset of direct double ionisation. The minimum energy of double ionisation is around 22 eV and therefore features below this energy are considered unphysical. The photon energy used for ionising C1s is 316 eV.

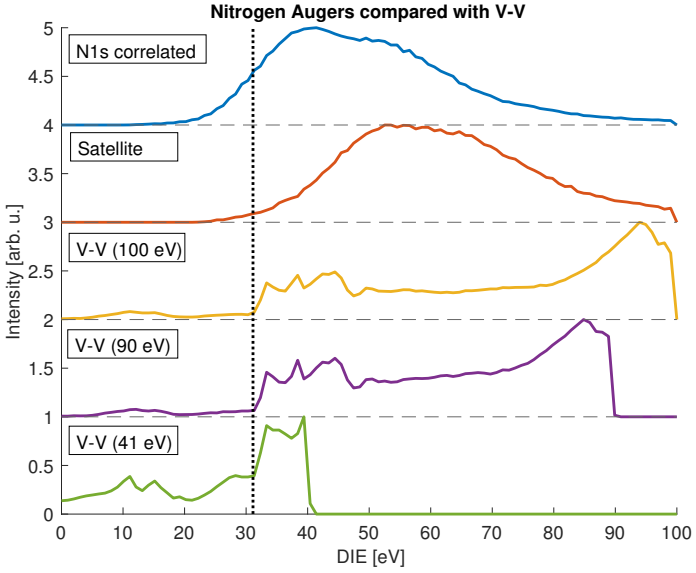

Figure 6.18: Comparison of the double ionisation spectra for the nitrogen Auger electrons and the valence-valence double ionisation spectra with a dotted line located at the onset of direct double ionisation. The minimum energy of double ionisation is around 22 eV and therefore features below this energy are considered unphysical. The photon energy used for ionising N1s is 426 eV.

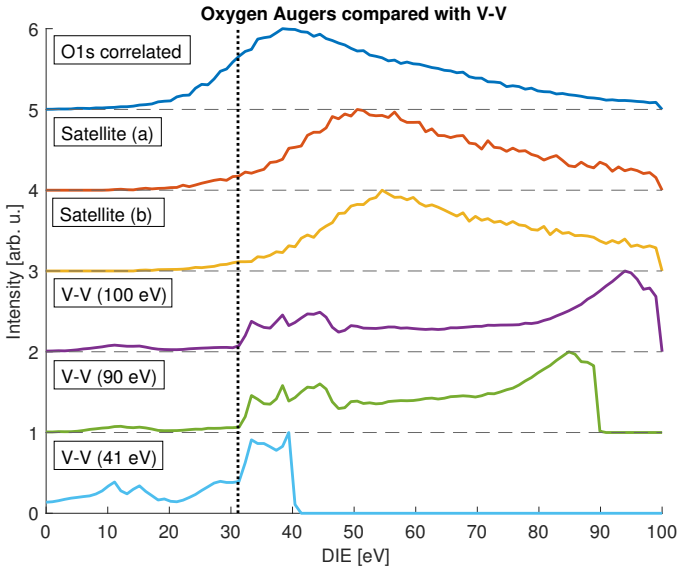

Figure 6.19: Comparison between the double ionisation spectra of the oxygen Auger electrons and the valence-valence double ionisation spectra with a dotted line located at the onset of direct double ionisation. The minimum energy of double ionisation is around 22 eV and therefore features below this energy are considered unphysical. The photon energy used for ionising O1s is 560 eV.

7
Conclusions & outlook

In this thesis the characteristics of the double ionisation of HNCO have been studied using the TOF-PEPECO method. For ionisation, a helium gas discharge lamp was used in the lab in Gothenburg and synchrotron radiation at the facility of BESSY-II. The processes studied are single ionisation, V-V and C-V direct double ionisation and double ionisation by the Auger route.

The valence single ionisation spectrum was studied using data from the Gothenburg lab and data from BESSY-II with retarded electrons. The spectra obtained are consistent with those published by J.H.D Eland [20]. Single ionisation was also used to check the purity of the sample.

The V-V direct double ionisation process was studied both in the Gothenburg lab and at BESSY-II, using different photon energies. The lower photon energy yielded better resolution but with the higher photon energies more structure for V-V could be identified. Five features were found in total, at the DIEs 34.0, 38.7, 42.7, 45.0 and 50.2 eV.

For C-V double ionisation, three cases were studied, where the core electron comes from the 1s core orbital for three different atomic sites: C1s, N1s and O1s. The C-V ionisation of the C1s-orbital has three peaks at the DIEs 317.8, 321.8 and 323.8 eV, C-V ionisation of N1s has two peaks at the DIEs 429.6 and 434.2 eV and O1s has three peaks at 561.6, 567.5 and 569.9 eV. The spectra for C-V were compared to the single valence photoionisation spectrum. The main expected difference between the two should be an offset corresponding to the energy required to eject the electron from the core and the core-valence interaction energy. Apart from the offset, the C-V spectra should look similar to the spectra for the single ionisation since the structure of the spectra is determined primarily by the valence electronic structure. The structure of the C1s C-V spectrum closely matches that of the valence spectrum, and from this an interaction energy of ~ 12 eV was extracted. However, we do notice there are pronounced differences between the C-V and single valence ionisation spectra for N1s and O1 ionisation. Thus the assumption that the only difference between the spectra is a shift in energy works well for carbon, but less well for the other two atomic species. To fully understand why this is the case, theoretical studies that model the core-valence process more completely are required.

The Auger process was also studied for the three cases where the 1s core electrons come from the three different atomic species and the energy distribution of the Auger electrons varied depending on which atom was studied. The spectra produced by the Auger processes were compared to the spectra of V-V direct double ionisation. The onset of double ionisation is compared between the two processes,

and it is possible to see that it is roughly the same. The onset energies should be comparable if the V-V and the Auger processes both lead to the ground state of the dication. The distributions are different in the two cases however, which is due to the fact that in the Auger process there are more possible routes and therefore the probability of ending up in the same final states varies when compared to V-V. The structure and onset of the Auger spectra, considering our low resolution, matches the results published by F. Holzmeier et al. [21].

Future work with the currently collected data is possible. The spectra and features identified in our analysis should be compared with theoretical quantum chemical calculations. The analysis could also be advanced by supplementary mass spectroscopy of HNCO using an electron-ion detection configuration for the spectrometer, which would allow the study of the final ion states of particular ionisation pathways and processes. The same type of experiments might also continue with other reactive molecules, such as HNCS, which has a more complex electronic structure due to the presence of sulphur. These types of studies of molecules such as HNCO may serve as a stepping stone to advance further in characterising short lived, highly reactive molecules.

Bibliography

[1] W. Farrar. Richard Laming and the coal-gas industry, with his views on the structure of matter. *Annals of Science*, **25**(3) 243–253 (1969). ISSN 0003-3790, 1464-505X. URL http://dx.doi.org/10.1080/00033796900200141

[2] J.J.Thomson. XL. Cathode Rays. *The London, Edinburgh, and Dublin Philosophical Magazine and Journal of Science*, **44**(269). ISSN 1941-5982. URL http://dx.doi.org/10.1080/14786449708621070

[3] *Report of the Board of Regents*, (The Institution, 1914). Google-Books-ID: ic0rAQAAIAAJ

[4] A. Einstein. Über einen die Erzeugung und Verwandlung des Lichtes betreffenden heuristischen Gesichtspunkt. *Annalen der Physik*, **322**(6) 132–148 (1905). ISSN 1521-3889. URL http://dx.doi.org/10.1002/andp.19053220607

[5] F. C. Jentoft, et al. Photoelectron Spectroscopy as a Tool for Studying Ceramic Interfaces: A Tutorial. In *Precursor-Derived Ceramics*, pp. 175–187, (John Wiley & Sons, Ltd, 2007). ISBN 978-3-527-61382-3. URL http://dx.doi.org/10.1002/9783527613823.ch15

[6] L. Meitner. Über die entstehung der β-strahl-spektren radioaktiver substanzen. *Zeitschrift für Physik*, **9**(1) 131–144 (1922). ISSN 0044-3328. URL http://dx.doi.org/10.1007/BF01326962

[7] P. Auger. The compound photoelectric effect. *J. Phys. Radium*, **6**(6) 205–208 (1925). URL http://dx.doi.org/https://doi.org/10.1051/jphysrad:0192500606020500

[8] C. Nordling, E. Sokolowski, and K. Siegbahn. Precision Method for Obtaining Absolute Values of Atomic Binding Energies. *Physical Review*, **105**(5) 1676–1677 (1957). ISSN 0031-899X. URL http://dx.doi.org/10.1103/PhysRev.105.1676

[9] D. W. Turner and M. I. A. Jobory. Determination of Ionization Potentials by Photoelectron Energy Measurement. *The Journal of Chemical Physics*, **37**(12) 3007–3008 (1962). ISSN 0021-9606. URL http://dx.doi.org/10.1063/1.1733134

[10] J. H. D. Eland and R. Feifel. *Double Photoionisation Spectra of Molecules*, (Oxford University Press, 2018). ISBN 978-0-19-878898-0. Google-Books-ID: yGdRDwAAQBAJ

[11] J.-L. Basdevant, J. Rich, and M. Spiro. *Fundamentals in Nuclear Physics: From Nuclear Structure to Cosmology*, (Springer Science & Business Media, 2006). ISBN 978-0-387-25095-3. Google-Books-ID: fO8rmQNxGZYC

[12] P. Thyssen and A. Ceulemans. *Shattered Symmetry: Group Theory From the Eightfold Way to the Periodic Table*, (Oxford University Press, 2017). ISBN 978-0-19-062017-2. Google-Books-ID: 3U0jDgAAQBAJ

[13] E. C. Stoner. LXXIII. *The distribution of electrons among atomic levels. The London, Edinburgh, and Dublin Philosophical Magazine and Journal of Science*, **48**(286) 719–736 (1924). ISSN 1941-5982, 1941-5990. URL `http://dx.doi.org/10.1080/14786442408634535`

[14] Vectr - Free Online Vector Graphics Editor. URL `https://vectr.com/`

[15] S. Andersson, et al. *Atom- och molekylfysik*, (Uppsala Universitet, 2005), second edition. ISBN 91-631-1595-6

[16] J. Liebig and F. Wöhler. Untersuchungen über die Cyansäure. *Annalen der Physik*, **96**(11) 369–400 (1830). ISSN 1521-3889. URL `http://dx.doi.org/10.1002/andp.18300961102`

[17] D. Cremer and E. Kraka. A description of the chemical bond in terms of local properties of electron density and energy. *Croatica Chemica Acta*, **57**(6) 1259–1281 (1984)

[18] Avogadro - Free cross-platform molecular editor. URL `https://avogadro.cc/`

[19] V. A. Rassolov, et al. The definition of core electrons. *Chemical Physics Letters*, **350**(5) 573–576 (2001). ISSN 0009-2614. URL `http://dx.doi.org/10.1016/S0009-2614(01)01345-8`

[20] J. H. D. Eland. The Photoelectron Spectra of Isocyanic Acid and Related Compounds. *Philosophical Transactions of the Royal Society of London. Series A, Mathematical and Physical Sciences*, **268**(1184) 87–96 (1970). ISSN 0080-4614. URL `https://www.jstor.org/stable/73970`

[21] F. Holzmeier, et al. Normal and resonant Auger spectroscopy of isocyanic acid, HNCO. *The Journal of Chemical Physics*, **149**(3) 034308 (2018). ISSN 0021-9606. URL `http://dx.doi.org/10.1063/1.5030621`

[22] N. Marcelino, et al. The puzzling behavior of HNCO isomers in molecular clouds. *Astronomy & Astrophysics*, **516** A105 (2010). ISSN 0004-6361, 1432-0746. URL `http://dx.doi.org/10.1051/0004-6361/200913806`

[23] J. A. Miller and C. T. Bowman. Kinetic modeling of the reduction of nitric oxide in combustion products by isocyanic acid. *International Journal of Chemical Kinetics*, **23**(4) 289–313 (1991). ISSN 1097-4601. URL http://dx.doi.org/10.1002/kin.550230403

[24] Assessment of the potential for isocyanic acid and other monoisocyanates to cause respiratory irritation and sensitisation (2009). URL https://www.semanticscholar.org/paper/ASSESSMENT-OF-THE-POTENTIAL-FOR-ISOCYANIC-ACID-AND/4c134cca512c5c4f3208b7cd28c58c7ce921f297#extracted

[25] J. Andersson. *Multi-electron processes in atoms and molecules*. Ph.D. thesis, University of Gothenburg (2019)

[26] P. Linusson. *Single-photon multiple ionization processes studied by electron coincidence spectroscopy*. Ph.D. thesis, Stockholms Universitet (2013). URL http://urn.kb.se/resolve?urn=urn:nbn:se:su:diva-89601

[27] L. Partanen. Auger cascade processes in xenon and krypton studied by electron and ion spectroscopy. *REPORT SERIES IN PHYSICAL SCIENCES*, **46** 57 (2007)

[28] A. Hult Roos. *Multi-Electron and Multi-Ion Coincidence Spectroscopy of Single-Photon Ionization Processes in Molescules*. Ph.D. thesis, University of Gothenburg (2019)

[29] E. Andersson. *Multi-Electron Coincidence Studies of Atoms and Molecules*. Ph.D. thesis, Uppsala University (2010). URL http://urn.kb.se/resolve?urn=urn:nbn:se:uu:diva-122811

[30] D. Attwood. *Soft X-Rays and Extreme Ultraviolet Radiation: Principles and Applications*, (Cambridge University Press, 2007). ISBN 978-0-521-02997-1. Google-Books-ID: clAANTKBStcC

[31] S. Plogmaker, et al. Versatile high-repetition-rate phase-locked chopper system for fast timing experiments in the vacuum ultraviolet and x-ray spectral region. *Review of Scientific Instruments*, **83**(1) 013115 (2012). ISSN 0034-6748. URL http://dx.doi.org/10.1063/1.3677329

[32] P. Kruit and F. H. Read. Magnetic field paralleliser for 2π electron-spectrometer and electron-image magnifier. *Journal of Physics E: Scientific Instruments*, **16**(4) 313–324 (1983). ISSN 0022-3735. URL http://dx.doi.org/10.1088/0022-3735/16/4/016

[33] O. Heaviside. XXXIX. On the electromagnetic effects due to the motion of electrification through a dielectric. *The London, Edinburgh, and Dublin Philosophical Magazine and Journal of Science*, **27**(167) 324–339 (1889). ISSN 1941-5982. URL http://dx.doi.org/10.1080/14786448908628362

[34] J. Ladislas Wiza. Microchannel plate detectors. *Nuclear Instruments and Methods*, **162**(1) 587–601 (1979). ISSN 0029-554X. URL http://dx.doi.org/10.1016/0029-554X(79)90734-1

[35] M. M. Coggon, et al. Emissions of nitrogen-containing organic compounds from the burning of herbaceous and arboraceous biomass: Fuel composition dependence and the variability of commonly used nitrile tracers. *Geophysical Research Letters*, **43**(18) 9903–9912 (2016). ISSN 1944-8007. URL http://dx.doi.org/10.1002/2016GL070562

[36] A. J. Gordon and R. A. Ford. *The chemist's companion: a handbook of practical data, techniques, and references*, (Wiley, 1972). Google-Books-ID: uyhRAAAAMAAJ

[37] O. Edqvist, et al. On the Photoelectron Spectrum of O2. *Physica Scripta*, **1**(1) 25–30 (1970). ISSN 1402-4896. URL http://dx.doi.org/10.1088/0031-8949/1/1/004

[38] A. Thompson, et al. *X-ray data booklet*, (Lawrence Berkeley National Laboratory, UNiversity of California, Berkeley, CA 94720, USA, 2009), third edition. URL http://xdb.lbl.gov/xdb-new.pdf

A

Appendix

A.1 Calibration using molecular oxygen in the Gothenburg lab

```
function [peakvalues, E_kin] = calibration_lab3(vector, data
    , hv, E_ion)
%Function using for 10 and 4 peaks of oxygen as calibration

%vector = a vector from 1 to number of elements in data,
    whole integers
%data = input data
%hv = photon energy
%E_ion = ionisation energy in eV

if numel(E_ion) == 10
    figure
    plot(vector, data)
    xlim([800 4700])
    [tof21,~] = ginput(10);
    close all

    peakvalues = tof21;
    E_kin=hv-E_ion;

elseif numel(E_ion) == 4

    figure
    plot(vector, data)
    xlim([600 900])
    [tof41,~] = ginput(4);
    close all

    peakvalues = tof41;
    E_kin=hv-E_ion;
else
    disp('Wrong number of peaks')
```

```
end

end
```

A.2 Calibration using argon at BESSY-II

```
function [peakvalues, E_kin] = calibration_bessy3(vector,
    data, hv)
%Function using Argon 248.63 eV and 250.78 eV as calibration

%vector = a vector from 1 to number of elements in data,
    whole integers
%data = input data
%hv = photon energy

figure()
plot(vector, data)
title('SPC')
xlabel('time [ns]')
ylabel('Counts per sec / intensity')

% zoom
[a,~] = ginput(2);
plot(vector, data)
xlim([a(1) a(2)])
title('SPC')
xlabel('time [ns]')
ylabel('Counts per sec / intensity')

% Pick out points
[tof,~] = ginput(2);
peakvalues(1,1)=tof(1,1);
peakvalues(2,1)=tof(2,1);

E_ion(1,1)= 248.63; %eV Argon peak 1
E_ion(2,1)= 250.78; %eV Argon peak 2

E_kin(1,1)=hv-E_ion(1,1);
E_kin(2,1)=hv-E_ion(2,1);

end
```

A.3 Fit a function to extract calibration parameters

```
function [fitted_function, constants] = get_parameters(
    peakvalues, E_kin)
%input: Time of flight and kinetic energy
%output: Fitted_function and parameters

ft = fittype('a.^2./(x+b).^2 + c');
fitted_function = fit(peakvalues,E_kin,ft,'startpoint',[1 1
    1]);

constants = coeffvalues(fitted_function);

end
```